*Human Brain Mapping*

WILEY

TECHNICAL REPORT OPEN ACCESS

# Event-Marked Windowed Communication: Inferring Activity Propagation from Neural Time Series

Varun Madan Mohan[1] | Thomas F. Varley[2] | Robin F. H. Cash[1] | Caio Seguin[3,4] | Andrew Zalesky[1,3]

[1]Department of Biomedical Engineering, Melbourne School of Engineering, University of Melbourne, Melbourne, Victoria, Australia | [2]University of Vermont, Burlington, Vermont, USA | [3]Department of Psychiatry, Melbourne Medical School, University of Melbourne, Melbourne, Victoria, Australia | [4]Department of Psychological and Brain Sciences, Indiana University, Bloomington, Indiana, USA

**Correspondence:** Varun Madan Mohan (vmadanmohan@student.unimelb.edu.au)

**Received:** 5 December 2024 | **Revised:** 20 April 2025 | **Accepted:** 22 April 2025

**Funding:** This work was supported by National Health and Medical Research Council, 2017527, Australian Research Council, DP170101815, FT220100091, University of Melbourne, and Rebecca L. Cooper Medical Research Foundation.

**Keywords:** connectome | functional connectivity | MEG | neural communication

## ABSTRACT

Tracking how activity or signal perturbations propagate in nervous systems is crucial to understanding interareal communication in the brain. Current analytical methodologies are not well suited to systematically infer interareal activity propagation from neural time series recordings. Here, we propose Event-marked Windowed Communication (EWC), a framework to infer activity propagation between neural elements by tracking the statistical consequence of spontaneous, endogenous regional perturbations. EWC tracks the downstream effect of these perturbations by subsampling the neural time series and quantifying statistical dependences using established functional connectivity measures. We test EWC on simulations of neural dynamics and demonstrate the retrieval of ground truth motifs of directional signaling, over a range of model configurations. We also show that EWC can capture activity propagation in a computationally efficient manner by benchmarking it against more advanced FC estimation methods such as transfer entropy. Lastly, we showcase the utility of EWC to infer whole-brain activity propagation maps from magnetoencephalography (MEG) recordings. Networks computed using EWC were compared to those inferred using transfer entropy and were found to be highly correlated (median $r = 0.81$ across subjects). Importantly, our framework is flexible and can be applied to activity time series captured by diverse functional neuroimaging modalities, opening new avenues for the study of neural communication.

## 1 | Introduction

Communication between neural elements—neurons, neural populations, and grey matter regions, plays a central role in the functioning of the brain. Understanding the principles by which signals are dynamically and flexibly transmitted in networked nervous systems remains an open challenge and active area of research (Avena-Koenigsberger et al. 2018; Kirst et al. 2016; Palmigiano et al. 2017). Efforts in this direction have produced a vast number of models of brain communication (Avena-Koenigsberger et al. 2018; Hahn et al. 2019; Seguin et al. 2023b), ranging from information transfer via neural oscillations (Bonnefond et al. 2017; Fries 2005, 2015; Hahn et al. 2014; Jensen and Mazaheri 2010) to network measures of connectome communication (Avena-Koenigsberger et al. 2019; Goñi et al. 2013; Seguin et al. 2018). Despite the abundance in models, efforts in model validation have been lacking, and it remains unclear which models faithfully

Caio Seguin and Andrew Zalesky are Joint senior authors.

describe empirical patterns of neural dynamics and signaling. A key barrier to progress in model validation is our current inability to infer events of signal transmission from recordings of neural activity. Current limitations in neuroimaging technology have seen activity propagation tracing often applied to smaller controlled stimulation experiments in microscale neuronal networks (Beggs and Plenz 2003, 2004; Lerner et al. 2016). Its application at the whole-brain scale is still limited (Griffa et al. 2017; Mitra and Raichle 2016; Shriki et al. 2013; Sorrentino et al. 2021), although approaches combining existing data to yield robust insights seem to show promise (Seguin et al. 2023a).

Determining how much of a signal, regional activity, or endogenous/exogenous perturbation is transmitted from one region to another across the underlying anatomical substrate can provide important insights into the principles of inter-areal communication and help validate existing computational models. Simply put, how a region "X" communicates with region "Y" can ideally be ascertained by gauging Y's activity in response to a perturbation in X. Extending this notion to instances over time, a series of perturbations of X may lead to a series of coupled responses in Y, resulting in a statistical dependence between the regions. Functional Connectivity (FC) can be used as a tool to assess this dependence. Broadly defined, FC quantifies statistical dependencies in time series of neural activity using measures such as the Pearson correlation or Mutual Information, capturing the extent to which the dynamics of two brain regions are synchronized over a period of time. Early investigations of FC saw its estimation on time series spanning entire scan durations, to reveal dominant and robust statistical associations between regions (Friston et al. 1993). This methodology was later extended to also capture statistical associations over smaller timescales within the scan by estimating FCs over subsamples of a scan typically defined by a sliding window, and termed dynamic FC (dFC) to distinguish it from its long timescale "static" counterpart (Hutchison et al. 2013; O'Neill et al. 2017; Vergara et al. 2019). Both dynamic and static FC estimation has seen extensive use in model formulation, validation as well as in experimental and clinical studies (Bazinet et al. 2021; Chapeton et al. 2019; Han et al. 2020; Hansen et al. 2015; Lynall et al. 2010; Palmigiano et al. 2017; Papadopoulos et al. 2020; Schipul et al. 2011; Schnitzler and Gross 2005; Shafiei et al. 2022; Suárez et al. 2020; Vázquez-Rodríguez et al. 2020). However, in systems exhibiting spontaneous, discrete, and directional signal transmission events, the statistical dependencies reflecting communication might be diluted or masked by segments of the signal with no relevance to communication, when static or dynamic FC estimation methods are employed. Information-theoretical measures such as Transfer Entropy stand to address this issue, but are typically data- and computation-heavy for whole-brain network inference (Novelli and Lizier 2021).

In this work, our aim was to develop an efficient method of inferring activity propagation patterns by combining the practicality and efficiency of undirected FC estimation with the dynamical resolution afforded by activity propagation tracing. We term this protocol Event-marked Windowed Communication (EWC). Specifically, EWC involves identifying salient events in neural recordings ("stimuli" or perturbations) and the subsequent estimation of the statistical dependence (FC) within short temporally ordered windows/subsamples of the signal, effectively capturing the response of downstream targets to these events. In this manner, EWC captures an indirect statistical analogue of activity propagation as opposed to spatiotemporally localized stimulation-response measurements. We first validate and demonstrate the utility of the EWC implementation using a simple *in silico* network motif with ground truth signaling embedded in its dynamics. We also show that the EWC approach allows us to use undirected FC measures to capture directional interactions. We then study the computational tractability of the approach by comparing network inference runtimes as a function of the number of nodes. Finally, we demonstrate a real-world application of the method on source-localized resting-state magnetoencephalography (MEG) recordings.

## 2 | Methods

### 2.1 | Dataset

Resting state MEG scans of 30 subjects (22–35 years, 17F), along with associated MEG anatomical data, 3T structural MRI data, and empty-room recordings, were obtained from the Human Connectome Project (Van Essen et al. 2013), through the ConnectomeDB platform. The MEG scans varied in duration from 5 to 6 min, at a sampling rate (SR) of 2035 Hz, and anti-aliasing low pass filtered at 400 Hz.

### 2.2 | Processing

The MEG scans were processed entirely using the MATLAB (The MathWorks Inc. 2022)-based Brainstorm software (Tadel et al. 2011), and in accordance with the pipeline described in Brainstorm's HCP-MEG tutorial (Niso et al. 2019). MEG recordings were first coregistered to the subject's structural MRI using the MEG anatomical data. A notch filter (60, 120, 180, 240, and 300 Hz), followed by high-pass filter (0.3 Hz), was applied to resting state and empty-room recordings to filter out power-supply and slow-wave/DC-offset artifacts respectively. Each subject's recording was then visually inspected, along with the channel power spectral density, to weed out bad channels and bad time segments. The ECG and EOG recordings were then used to identify heartbeats and eye-blinks, after which associated artifacts were removed using their signal space projections (SSPs) (Uusitalo and Ilmoniemi 1997).

The source-level activities at 8000 points, defined by the fsLR4k mesh, were then estimated from the sensor-level recordings. This involved first computing the head model using overlapping spheres and constrained dipoles normal to the cortical surface and estimating the noise covariance from the empty-room recordings. Source-level activities were then estimated using the dSPM method (Dale et al. 2000) available in Brainstorm. The sources were then parcellated using the Schaefer-Yeo 7-network 100 atlas (Schaefer et al. 2018), with the parcel activity computed as the principal component of the constituent source activities.

The centroid coordinates of the Regions of Interest (ROIs) were used to define a Euclidean distance (ED) matrix between all possible pairs of regions (Abeysuriya et al. 2018; Deco et al. 2009;

Papadopoulos et al. 2020). Inter-regional distances were proportionally converted to time delays ($\delta$) as

$$\delta_{ij} = ED_{ij} / v$$

where $v$ is the conduction velocity (CV) of neural signals, set to 10m / s (Papadopoulos et al. 2020).

Parcellated source-localized resting-state MEG recordings were corrected for source leakage effects by removing zero-lag correlations as per (Colclough et al. 2015), using the OHBA Software Library (OSL) package in Python (Quinn et al. 2023).

## 2.3 | Estimating Inter-Areal Communication

Inter-areal communication was inferred from the source-level parcellated time series using two approaches—a conventional FC-based approach, and Event-marked Windowed Communication (EWC). We use the suffix "-Full" after the FC measure to indicate a conventional estimation technique, and "-EWC" to indicate our implementation. Prior to estimation, source-level parcellated time series were first epoched into 10$s$ segments, epochs that contained bad segments were removed, and each epoch was then processed independently.

### 2.3.1 | "-EWC" Implementation

We developed EWC to quantify functional interactions between neural elements following discrete signaling events or perturbations in their activity time series. The EWC protocol is composed of three main elements: (1) event-identification, (2) temporal ordering based on conduction delays, and (3) estimation of the FC between event-marked windows/subsamples (Figure 1). Event-identification involves identifying salient features or instances where activities notably deviate from typical behavior. We did this by z-scoring the data within an epoch: This helped identify the spread of regional activities around their respective mean behaviors. For all regions, the timepoints at which the $|z| > 3$ were identified as "supra-threshold events" (for brevity, we will refer to them

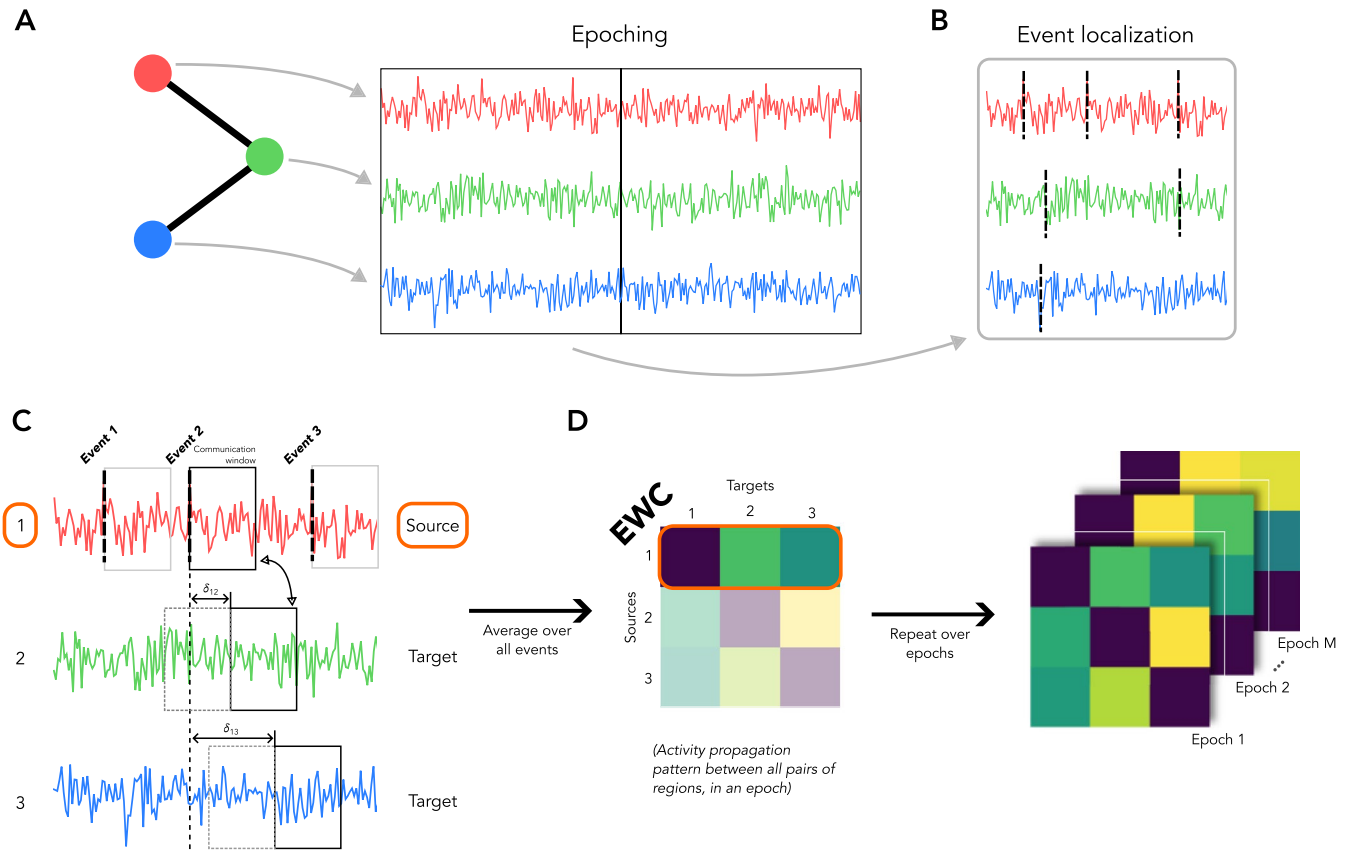


**FIGURE 1** | A pipeline to estimate communication patterns from regional time series. (A) Regional activities are divided into epochs of fixed length, and each epoch is processed independently. (B) For each epoch, the regional activities are individually z-scored to identify instances of deviation from mean behavior, which are termed "supra-threshold events". (C) Each region is successively chosen as a "source". For each event of a source, a communication window that encompasses the activity over a duration of 1 s, is defined starting at the time point of the event. Similar communication windows are defined over the activities of all other regions (termed "targets"), starting at timepoints delayed with respect to the source event, in proportion to the Euclidean distance between the source and target. (D) For each event for a chosen source, the Event-marked Windowed Communication (EWC) is estimated between the source and all possible targets by computing the functional connectivity between the activities contained in the communication windows of the source and target. The past activity of the target is used as the conditioning variable. The pairwise EWC values over all events of a source (within an epoch) are averaged, to populate a row of the EWC matrix corresponding to the source index. Steps (B–D) are repeated over all epochs to give epoch-level EWC matrices that capture the dynamic communication patterns over the entire scan duration.

as "events" for the remainder of this paper). A high z-score threshold selects significantly strong deviations, or perturbations, which we argued was more likely to cause measurable downstream effects on the activity of the rest of the brain, than smaller fluctuations. Finite signal conduction times would additionally imply that these downstream effects be delayed. We focused the estimation of inter-areal communication to a segment of the time series—termed a "communication window", spanning a duration of 1 s, starting at the event timepoint for the source, and at a future timepoint for a target (temporal ordering based on inter-areal distances). Once the temporally ordered communication windows were defined, the downstream effect of the signaling event was quantified by the statistical association between the within-window activity time series of the source and target. EWC is flexible and this association can be computed using various measures of FC, such as the partial correlation (PC) or conditional Mutual Information (cMI).

Specifically, following event identification, the following steps were executed iteratively over all ROIs for each event:

1. A region was chosen as a source, and a window of $1s$ was defined starting at the event. Any additional events that fell within this window were removed and not considered in the subsequent iterations, to avoid excessive computation. The window length was chosen to be short enough to capture the immediate effects of the communication events and minimize contributions from internal dynamics.
2. A window of similar length was placed at the time series of all other ROIs (targets) within the same hemisphere, at timepoints delayed in proportion to the Euclidean distance between the source and the target (see Processing). The $1s$ length of the window can also accommodate the effects of source signals travelling at velocities much slower than $10m/s$ (used in the calculation of inter-regional delays).
3. The FC measure (PC, cMI) was computed between all pairs of the source and target signals within the respective windows, conditional upon the target's immediate past activity over the duration of one window, up to the event. This conditioning was done to remove biases due to internal dynamics (not associated with communication). The FC estimates were checked for significance, with a Bonferroni-corrected threshold of $\alpha = \frac{0.01}{N_{\text{events}}}$ ($N_{events}$ is the total number of events within the epoch), since we test the correlation multiple times within an epoch. For $p$-values above this threshold, the estimates were set to zero. The final measure is termed the Event-marked Windowed Communication (EWC).
4. The event-level EWC values from the source to all possible targets were then averaged to yield the source's epoch-level EWC.

Once the above steps were completed for all possible sources, we were left with an epoch-level $N \times N$ EWC matrix that captured the communication between all source-target pairs, averaged over all the events in the epoch. For a given subject whose scans were divided into $M$ epochs, the communication protocol yields an $N \times N \times M$ EWC matrix over the entire scan duration. This matrix was then averaged across epochs to give the subject-level EWC matrix. The averaging carried out across events in an epoch, and then across epochs, minimises the contribution of spurious FC estimates between source-target pairs.

#### 2.3.2 | "-Full" Implementation

In the conventional approach, the FC was computed in a pairwise manner, between all regions, between the entire epoch time series. Each FC estimate was significance tested with a threshold of $\alpha = 0.01$. Like the EWC implementation, the pairwise FC was computed for all epochs, yielding an $N \times N \times M$ matrix (for $M$ epochs) over the entire scan duration.

### 2.4 | Demonstration on a Network Model

In order to identify the merits and limitations of our approach prior to its application to neuroimaging data, we tested it on the activities of a four-node system with Linear Stochastic Model (Galán 2008) dynamics. The dynamics of a node $i$ is described as:

$$\dot{x}_i = -x_i + K \sum_{j \in N} C_{ij} x_j \left(t - \delta_{ij}\right) + \sigma \mathcal{N}(0,1)$$

where $C_{ij}$ is the connectivity strength between nodes $i$ and $j$, $K$ is a global coupling parameter ($K = 1$), $\delta_{ij}$ is the time delay between $i$ and $j$ (proportional to the Euclidean distance), $\mathcal{N}(0,1)$ denotes random standard normal noise, and $\sigma$ is the noise amplitude. Three of the nodes were connected in a linear chain-like topology, and the fourth node was isolated from the rest of the system: $C_{12} = C_{21} = C_{23} = C_{32} = 1;\ C_{13} = C_{31} = 0;\ C_{4i} = C_{i4} = 0\ \forall\ i \in \{1,2,3\}$.

In addition to the LSM dynamics, a Poisson process caused both the terminal nodes to "pulse" randomly, with an average frequency $\nu$, and with a pulse amplitude of 0.1. This resulted in the dynamics of the central node to be a mix of its internal dynamics, and random inputs from the two terminal nodes. While Poisson spiking is a convenient means of exercising control over ground-truth signaling, it can result in an inflation of nodes' mean activities from the "baseline" at high $\nu$, due to rapid fluctuations.

The communication protocol was tested across systematic variations of $\sigma$, $\delta_{23}$, and $\nu$.

For each set of parameter values, we simulated the dynamics for 205s, at a sampling rate of 2035Hz, using an Euler integrator. Epoch duration and communication window durations were set to $10s$ and 1s respectively. Twenty trials of each simulation were carried out.

Communication was inferred using the Full implementation of Transfer Entropy (TE) and bivariate Granger Causality (GC) (TE-Full and GC-Full), and EWC implementation of conditional

Mutual Information (cMI) and Partial Correlation (PC) (cMI-EWC and PC-EWC), on the activity time series of all four nodes. We assessed the ability of the tested methods to resolve accurate communication patterns by determining the discernibility of their true and false connections (with respect to the ground truth) that is, how different the estimate from $1 \to 2$ and $3 \to 2$ (true) is from $4 \to 2$ (false), and forward and reverse connections that is, $1 \to 2$ versus $2 \to 1$. We did this by estimating the standardized contrast, computed as the difference between the relevant estimates, normalized by their pooled standard deviation. A non-zero contrast value quantifies the discriminability between estimates.

## 2.5 | Computation Time Benchmarking

To compare the computation times for different protocols as a function of network size, activity propagation was inferred as TE-Full, MI-Full, cMI-EWC, and PC-EWC for time-series data of $200s$. To ensure that the estimated computation times were realistic, the recordings were randomly sampled source localized MEG recordings (see Section 2.2). The following steps were repeated for a network size $N$ (for 10 trials):

1. $N$ regions are randomly chosen, and the associated regional time series were trimmed to $200s$ (sampling frequency$=$ 2035Hz).
2. Inter-regional delays were set to $0.015ms$.
3. Activity propagation was estimated between all pairs of regions as TE-Full, MI-Full, cMI-EWC, and PC-EWC.
4. Repeat with a new random selection of regions.

## 2.6 | Partial Correlation

The partial correlation (PC) quantifies the linear association between two random variables, while discounting the effects of a third variable. In the EWC implementation, we set the third variable as the target's past over a single window duration, up to the timepoint of the event. We compute the PC using MATLAB's "partialcorr" function. The significance level was set to $\alpha = \frac{0.01}{N_{\text{events}}}$. The partial correlation is a continuous function varying from $-1$ to 1, indicating a perfectly negative to perfectly positive linear correlation respectively.

## 2.7 | Conditional Mutual Information

The conditional Mutual Information (cMI) is an information theoretic measure that quantifies the shared information between random variables (representing regional activities) in the context of the activity of some exogenous additional regions (represented as a conditioning variable). It is a variant of the widely used Mutual Information (MI) (Hulata et al. 2002; Novelli and Lizier 2021; Palus 1997; Wilmer et al. 2012).

Given random variables $X$ and $Y$, containing the activities of two regions, and a third random variable $Z$, containing the activity of a third region (or a set of multiple regions), the cMI is measured in terms of entropies as:

$$I(X;Y|Z) = H(X|Z) + H(Y|Z) - H(X,Y|Z)$$

where $H(X|Z)$ and $H(Y|Z)$ are the conditional entropies associated with variables $X$ and $Y$, and $H(X,Y|Z)$ is the conditional joint entropy.

The cMI is a symmetric measure, that varies from 0 when the two random variables are independent of each other, to $\infty$ when they are identical.

The target's past activity was used as the conditional variable to remove any biases to the measured communication from internal dynamics.

## 2.8 | Granger Causality

Granger Causality (GC) is a measure of statistical predictability that quantifies how well the behavior one variable forecasts another (Bressler and Seth 2011; Granger 1969). Defined in the domain of Vector Autoregressive (VAR) processes, the bivariate GC quantifies the difference in prediction error when a univariate VAR(p) model is used to model a region X's activity versus when X's activity is modeled using a bivariate VAR(p) model that includes the past of another region Y (the "cause"). If the inclusion of the past of Y results in a better prediction of X's activity than through X's past alone i.e., if the prediction error when using the bivariate VAR(p) model is lower than when the univariate model is used, Y is said to "Granger cause" X. For an accurate and meaningful GC estimate, choosing an optimal lag value for the VAR(p) processes, p, is essential. For empirical data, this is achieved by fitting models of increasing lag to the data, estimating an information criterion like the Akaike Information Criterion (AIC), and finding the model order associated with minimal AIC.

For two stochastic and wide sense stationary variables $\mathbf{X}$ and $\mathbf{Y}$, the regression of the values of $\mathbf{X}$ onto a univariate and bivariate VAR(p) model, termed the restricted and unrestricted models, is given as:

$$X_t = A \bullet X_{t-1}^{(p)} + \varepsilon_t \text{ (Restricted)}$$

$$X_t = A' \bullet \left( X_{t-1}^{(p)} \bigoplus Y_{t-1}^{(p)} \right) + \varepsilon_t' \text{ (Unrestricted)}$$

where $p$ is the model order, $X_{t-1}^{(p)}$ is the vector of past values of $\mathbf{X}$ up to the model order $\{X_{t-1}, X_{t-2}, \dots, X_{t-p}\}$, $\bigoplus$ represents the concatenation of vectors, $A$ and $A'$ contain VAR model coefficients, and $\varepsilon_t$ and $\varepsilon_t'$ are the prediction errors. The bivariate GC between $\mathbf{X}$ and $\mathbf{Y}$ is then defined as:

$$\mathcal{F}_{X \leftarrow Y} = \ln \frac{\text{var}(\varepsilon_t)}{\text{var}(\varepsilon_t')}$$

Bivariate GC was estimated using the computationally efficient state-space approach (Barnett and Seth 2015) implemented in the Multivariate Granger Causality (MVGC) toolbox (Barnett and Seth 2014). Based on the AIC, the optimal model order in the network model was chosen as 1, and for the empirical resting-state MEG recordings, the AIC monotonically reduced

with increasing model order and plateaued around an order of 50. A more parsimonious model order of 40 (corresponding to a lag of approx. 19 ms) was then chosen.

### 2.9 | Transfer Entropy

The Transfer Entropy (TE) is a widely used information-theoretic measure of directional influences (Kirst et al. 2016; Novelli et al. 2019; Novelli and Lizier 2021; Palmigiano et al. 2017; Schreiber 2000; Shorten et al. 2021). Specifically, for two random variables X and Y, it quantifies how much uncertainty in the future of Y (target) is reduced through the knowledge of the past of X (source), conditional on the past of Y. It is technically a special case of the cMI, where the shared information is estimated between relatively time-shifted random variables:

$$TE_{X\to Y}(k,l,\delta) = I\left(X^{(l)}_{t+1-\delta}; Y_{t+1} \middle| Y^{(k)}_{t}\right)$$

where $X^{(l)}_t = \{X_{t-l-1}, \dots, X_{t-1}, X_t\}$, and $\delta$ is the causal delay. There are multivariate variants of the TE, which also condition it on other possibly mediating variables. In this work, we use its simplest form—the bivariate TE. Multivariate forms of the TE are generally better than other techniques at capturing ground truth asymmetries but are considerably more data- and computation-intensive (Novelli and Lizier 2021).

As mentioned above, the TE is a special case of the cMI, because of which our implementation of the cMI between the source and target, conditioned on the target's past, is closely related to estimating the TE between the regions, albeit within the event-marked communication windows. This is captured in their respective formulae:

$$^{\text{Full}}\text{TE}_{X\to Y} = I\left(X_t; Y_{t+\delta+1} \middle| Y_{t+\delta}\right),\ \ t \in \{1, 2, \dots, T-\delta-1\}$$

$$^{\text{EWC}}cMI_{X\to Y} = I\left(X_{e+t-1}; Y_{e+t+\delta-1} \middle| Y_{e+t+\delta-win-1}\right),\ \ t \in \{e, e+1, \dots, \text{win}\}$$

where $e$ is the timepoint of an event, and win is the length of a window.

We used the Gaussian estimator in the Java Information Dynamics Toolkit (JIDT) (Lizier 2014) to compute all information theoretic quantities. Using the Gaussian estimator allowed each estimate to be significance-tested analytically from the $\chi^2$-distribution. The estimators were run with default properties, except for the source-destination delay in the TE estimator, which was changed from the default value of 1, to the Euclidean distance-based inter-regional delay (see Processing). All information theoretic quantities (including the EWC) are measured in nats.

## 3 | Results

The analyses of this paper can be divided into three main sections. First, we tested our method in simulated time series produced by a simple connectivity motif in which node activity was governed by Linear Stochastic Model (LSM) dynamics (Figure 2A). The simple dynamical landscape of the LSM allowed us to impose ground truth signaling between nodes. We assessed our method's ability to identify these communication patterns in relation to previously proposed measures of FC. Second, we estimated the computational costs associated with the EWC protocol and benchmarked it against commonly employed FC estimation methodologies. Third, we applied our method on source localized MEG recordings and gauged the agreement between activity propagation (FC) inferred via EWC and bivariate Transfer Entropy.

### 3.1 | Asymmetric Signaling Over a Network Motif

We tested the EWC protocol in a four-node motif (Figure 2A) with Linear Stochastic Model (LSM) dynamics and Poisson spiking to emulate punctual events of directional signaling (see Section 2). EWC was implemented using two measures of within-window FC—partial correlation (PC-EWC) and conditional mutual information (cMI-EWC). Note that traditionally, these are symmetric measures that cannot resolve the directionality of functional interactions. We benchmarked EWC against Transfer Entropy (TE-Full), which was conventionally estimated based on the entire time series. We compared the ability of these measures to retrieve the ground truth signaling motif in simulations with increasing noise levels. To enable comparison of the different measures, we estimated the standardized contrast between the FC in true (existing: between nodes 1, 2 and 3) and false (absent: between nodes 4 and 2) connections, as well as in the forward ($1\to2$) and reverse ($2\to1$) directions. A standardized contrast of zero signifies no discernible difference between estimates.

We considered the performance of our method as a function of the ratio between the noise level in the system and the amplitude at which the source regions pulsate. The delay between the sources (nodes 1, 3, and 4) and the target (node 2) was set at $15ms$, and the sources pulsated according to a Poisson process with a mean frequency of 0.2Hz (Figure 2A). The ground truth connections were between nodes 1 and 2, and 3 and 2, with no outgoing or incoming connections from node 4, by construction (See Section 2.4). Additionally, the spiking behavior in nodes 1 and 3 would imply an asymmetric influence from them to node 2. We observed that estimating the TE-Full resulted in a good representation of the ground truth, with strong interactions from nodes 1 and 3 to 2 (Figure 2C). Importantly, the corresponding contrast distribution indicated that the interaction between node 4 (isolated) and 2 could be clearly discriminated from the true interactions, providing evidence of good specificity (Figure 2F). When the FC was instead measured using cMI-EWC, we observed an interaction between regions 4 and 2, although this false positive interaction was considerably weaker than the ground truth interactions from node 1 to 2, and 3 to 2, particularly at low noise levels (Figure 2D). Interestingly, PC-EWC performed well when compared to cMI-EWC. Like TE-Full, PC-EWC also resulted in a good representation of the ground truth (Figure 2E). The contrast between estimated interactions showed that true connections could be distinguished from absent connections even at large levels of noise (Figure 2H), although not as well as TE-Full. Importantly, in the case of cMI-EWC and PC-EWC, asymmetric interactions were estimated, despite the FC measures

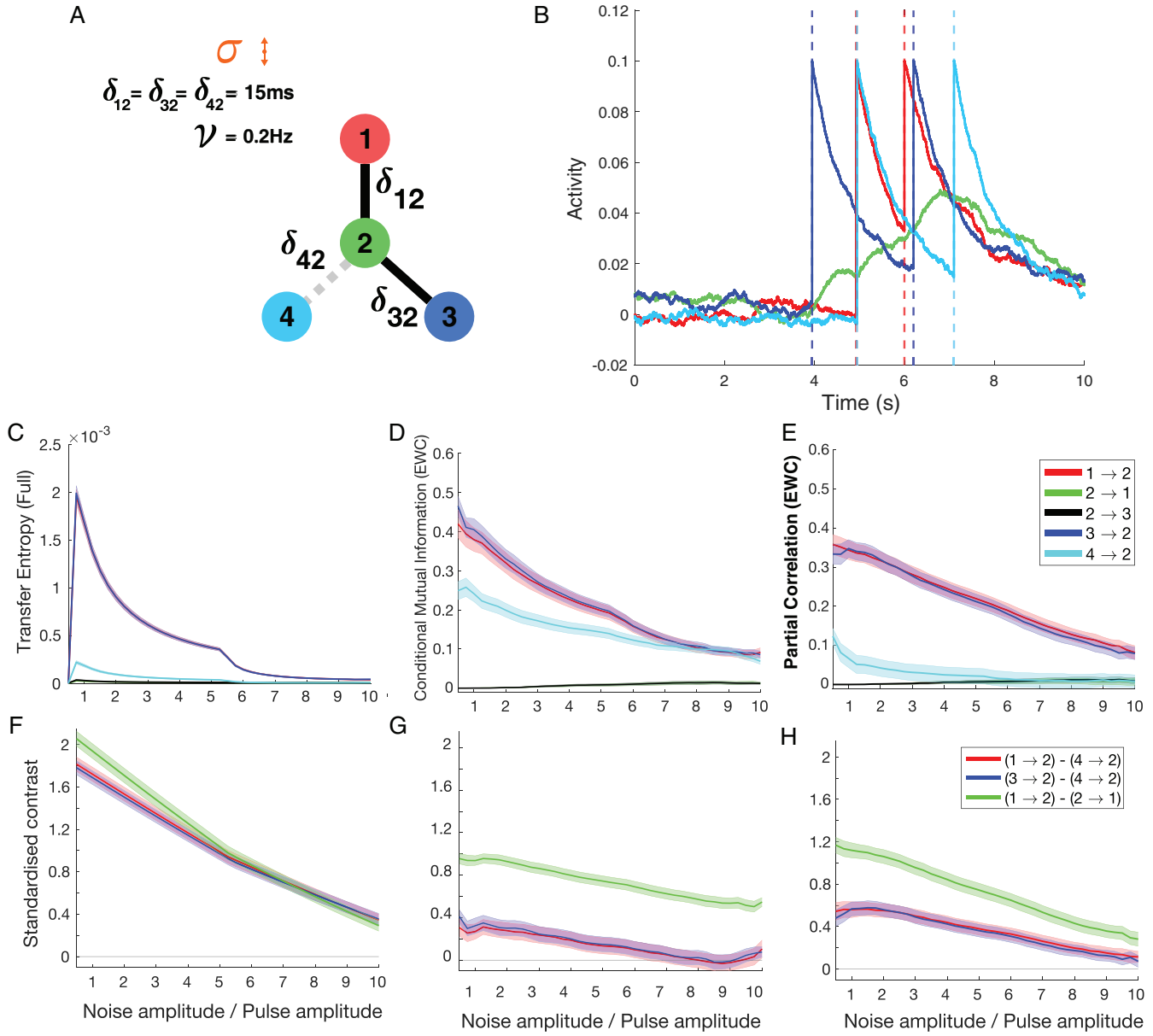


**FIGURE 2** | Communication over a network motif. (A) We test our method of estimating communication patterns on a simple 4-node network motif with three connected nodes (nodes 1, 2, and 3) and an isolated node (node 4). The solid black edges and the dashed grey edge indicate the presence and absence of a ground truth connection respectively. The activities of the individual nodes in this network are described by a Linear Stochastic Model. The dynamics of the red, blue and cyan nodes have an additional Poisson process, causing it to spike at an average rate of 0.2 Hz, emulating communication events. $\delta_{xy}$ is the delay between nodes $x$ and $y$, in *ms*. The noise amplitude of the LSM, $\sigma$, is varied relative to the fixed Poisson pulse amplitude of the sources. (B) 10*s* of simulated activity of the network in (A). The dashed lines at the location of the pulses mark communication events used in the EWC protocol. Note that in addition to nodes 1 and 3, events are detected in node 4 as well, based on its pulses. (C) Transfer entropy (in nats) between nodes, estimated over the full signal. (D) Conditional Mutual Information (in nats) between nodes, estimated as per the EWC protocol (E) Partial Correlation (Pearson-R) between nodes, estimated as per EWC. We show only the absolute correlation strengths. (F–H) Standardized contrast (difference between FC estimated between of True and False connections that is, solid and dashed edges in (A), normalized by their pooled standard deviation) plots associated with the FC estimates. A non-zero contrast value quantifies the discriminability between estimates. Shading in the plots represent ± SEM (20 trials). All plots maximally smoothed (i.e., using all available points) to clearly reveal trends.

being undirected/symmetric. This asymmetry is a result of the temporal ordering within the EWC implementation.

To further contextualize EWC's performance in gauging the true network communication structure, we employed another established directed FC methodology—the Bivariate Granger Causality (GC-Full), which was estimated on the entire time series. Like TE-Full, GC-Full also produced an accurate representation of the ground truth interactions of the constructed system (Figure S5A).

Additionally, we also tested whether a common source equidistant from two targets would result in a spurious functional link between them (a closed triangle problem). For this, we set

region 2 as the pulsating source and estimated the PC-EWC. We observed that our method correctly identified communication from node 2 to both 1 and 3, with negligible communication in the opposite direction or between the targets (Figure S1). We also tested the EWC implementation over a range of conduction delays and mean firing rates of the sources (Figure S2).

To summarize, our comparative analyses demonstrate that EWC can accurately capture directional interactions over a range of noise levels, delays, and firing rates. We emphasize that PC and cMI, being undirected/symmetric measures, were only able to capture directional signaling due to the temporal ordering implemented by the EWC protocol. Despite these positive results, based on our observations of the standardized contrast, we find that TE-Full still provides the strongest discriminability between the absence and presence of signaling patterns. For this reason, we continue using TE-Full as a representative benchmark of directed FC in the subsequent analyses.

### 3.2 | Computational Tractability of the EWC Protocol

An important consideration for any analysis pipeline, particularly if applied in an exploratory context, is its computational tractability. The EWC protocol involves two main computational segments—first is the event identification step, and the second is the estimation of statistical dependence (through FC) to infer activity propagation. Since some of the FC estimation methods, particularly those involving nonparametric information theoretic functions, are computationally intensive to begin with, the computational implications of adding additional components must be explored. In this section, we compared the computational tractability of the EWC protocol to full versions of TE and MI, and EWC versions of the cMI and PC. We used these methods to estimate functional/activity-propagation networks comprising an increasing number of nodes. Nodal time series were sampled from source-localized MEG recordings (see Section 2).

As expected, the computation time increased with network size in all cases. Interestingly, despite the increased number of computations—event identification and multiple FC estimations (for each event), the EWC was found to be computationally less intensive than TE-Full. Specifically, for the chosen parameters, PC-EWC took approx. 75% less time than TE-Full, and cMI-EWC took approx. 45% less time. Since cMI-EWC is closely related to TE-Full (see Section 2), but estimated over shorter windows, it shows that the computational efficiency of the EWC protocol can be largely attributed to the subsampling, despite it increasing the overall number of computations. Although the method chosen would have to ideally suit the research problem, this analysis and the visualization presented in Figure 3 nevertheless helps benchmark the computational cost of the EWC protocol against established methodologies in resting state analysis.

In short, we find that both methods of estimation (Full or EWC) and the within-window FC measure affect computation time. Importantly, using the EWC protocol generally leads to a decrease in computation time. In addition, the gain in computational time grows as a function of network size, indicating that

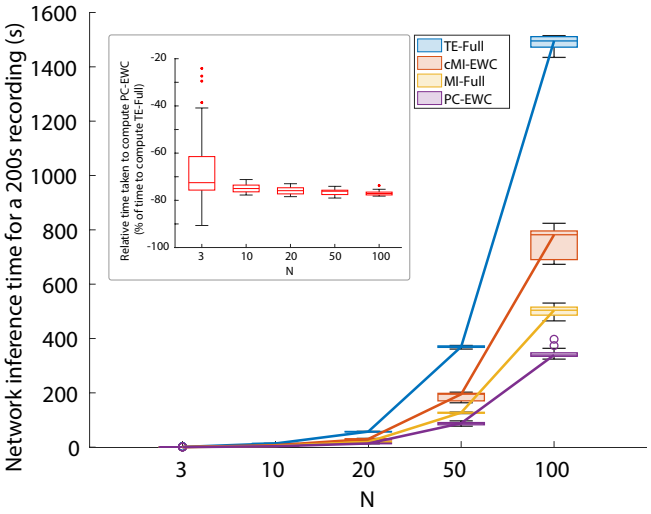


**FIGURE 3** | Time taken for network inference as a function of network size. Signals spanning 200*s* (Twenty 10*s* epochs) sampled from source-localized MEG recordings of three subjects. Sampling repeated 10 times per subject for each network size (each box plot spanning 30 data points). Circles represent outliers. (Inset) Percentage of time taken to compute PC-EWC, relative to the time taken to compute TE-Full. For a range of network sizes, PC-EWC takes ≈75% less time to compute for a 200*s* scan, or equivalently, is ≈4 times faster.

EWC may confer pronounced benefits for the estimation of fine-grained functional networks (e.g., > 1000 nodes). Combined with our results from the previous section, we find that PC-EWC can be computed ≈4 times faster than TE-Full, while also resolving asymmetries in signaling.

### 3.3 | Inferring Whole-Brain Activity Propagation Patterns From MEG Recordings

Having benchmarked both the computational efficiency of the EWC protocol and the accuracy of inferred activity propagation maps against conventional FC estimation methodologies *in silico*, in our final set of analyses, we tested the agreement between EWC and TE maps derived from empirical neuroimaging data. Specifically, we computed PC-EWC and TE-Full on minimally pre-processed resting-state source-localized MEG recordings of 30 subjects from the Human Connectome Project (HCP) (left-hemisphere results in main text, right-hemisphere results Figure S3). The temporal ordering was based on delays proportional to the inter-regional Euclidean distance (see Section 2).

For each subject, we computed the correlation between the PC-EWC and TE-Full matrices and found that the two measures led to highly correlated estimates of functional connectivity (Figure 4B). The median correlation coefficient across subjects was $r \approx 0.82$ ($p < 0.0001$) (Figure 4C top). Notably, the subsampling of the EWC protocol led to a significantly quicker inference of activity propagation (Figure 4C bottom). In addition to the high subject-level agreement, the EWC implementation also allows us to study how signaling directions and strengths change across the scan, by estimating the degree of asymmetry and variance of estimates at different scales (event-, epoch-, and subject-levels) (Figure S4).

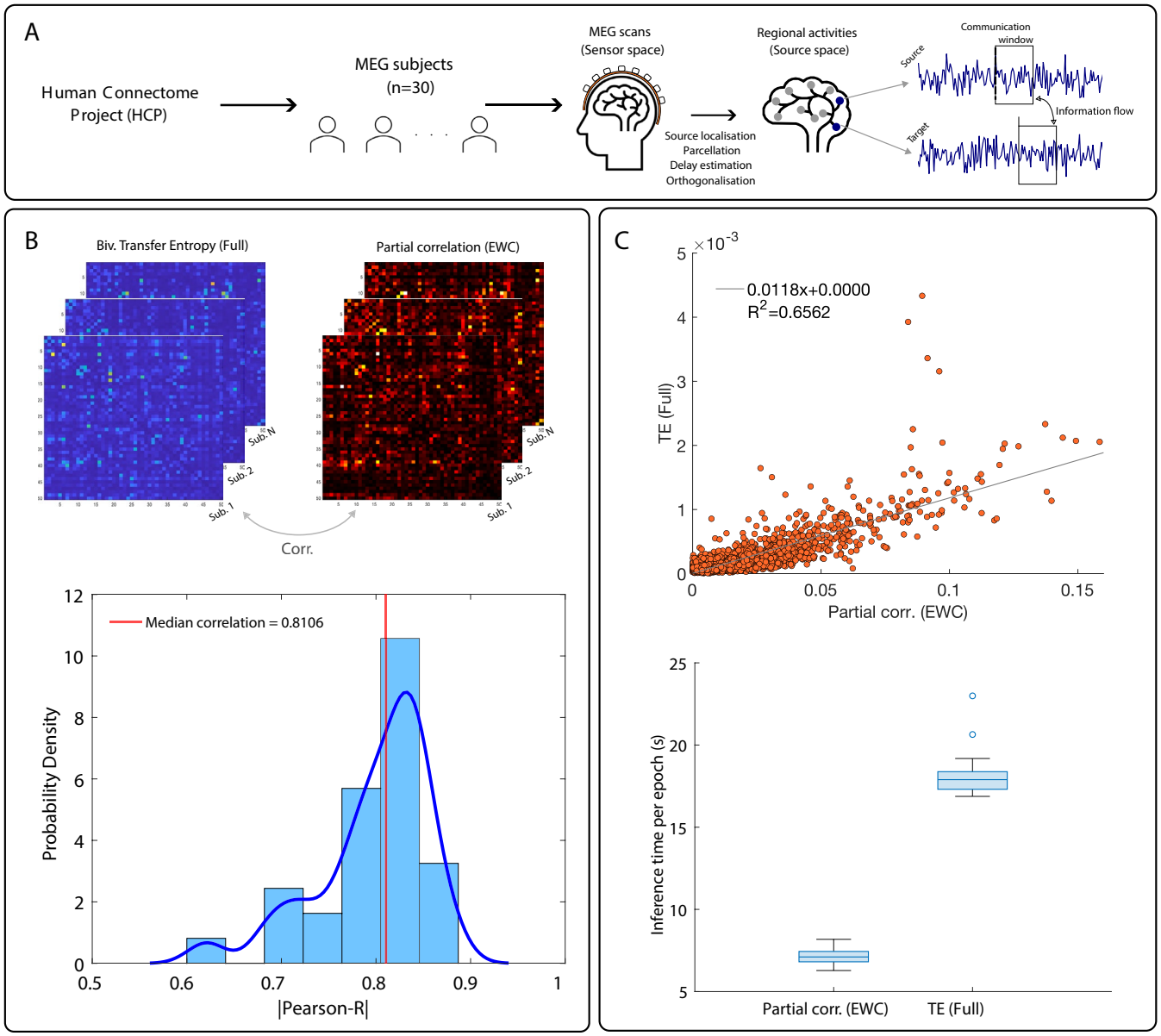


**FIGURE 4** | Application of EWC on source-localized MEG recordings. (A) Resting-state MEG scans of 30 subjects from the Human Connectome Project (HCP) were pre-processed, source localized, orthogonalized, and epoched into 10 s segments. (B) (Top) The subject-level FC for the left hemisphere was estimated as PC-EWC and TE-Full. (Bottom) Edgewise correlation distribution between the subject-level FC matrices. The red line marks the median correlation. (C) (Top) Scatterplot of edge weights for a representative subject (closest to the median correlation). Correlation after excluding outliers (> 4 standard deviation) – $r \approx 0.87$, $p < 0.0001$. (Bottom) inference time per epoch across subjects, for each of the methods.

Although TE is an established means of gauging directed interactions as demonstrated in Figure 2, and enables straightforward comparison with PC-EWC, we additionally benchmarked the communication maps inferred using EWC to estimates using Bivariate Granger Causality (GC-Full). Bivariate Granger Causality captures asymmetric influences based on the relative autoregressive predictability between regional activities, as opposed to the information theoretic approach of TE, allowing for a more comprehensive empirical assessment of EWC. Notably, we observed a strong correlation between PC-EWC and GC-Full, comparable to its agreement with TE-Full (Figure S5B).

To summarize, in this section we demonstrate a real-world application of the EWC to capture activity propagation patterns from resting state MEG recordings using PC-EWC. We show that activity propagation inferred through FC as per the EWC protocol shows good agreement with our conventional reference using the TE, while being considerably less computationally intensive. This lends support to EWC as a viable technique for studying how activity or endogenous perturbations flow between functional entities, particularly when multiple functional components are involved.

## 4 | Discussion

Understanding how the brain routes information is an open problem in neuroscience with crucial implications to our knowledge of perception and cognition. In this work, we focus

on the first step towards addressing this problem—reliably inferring communication from neuroimaging data. We introduce a time series analytical technique, termed Event-marked Windowed Communication (EWC), to capture dynamic statistical relationships driven by inter-regional communication. This method captures the inter-regional propagation of discrete signaling events or endogenous perturbations using functional connectivity (FC) measures estimated on select subsamples of the signal. We demonstrated the merits and limitations of this method *in silico*, using different FC measures, and compared it to established methods of inferring directional relationships (Figure 2). We then applied it to source-localized MEG data, where high correlation was evident between subject-level FC patterns derived using EWC and widely used directed FC approaches like Transfer Entropy (TE) (Figure 4) and Bivariate Granger Causality (Figure S5). Importantly, we also showed that the EWC protocol is computationally efficient (≈2.5 times faster per 10s-epoch when using the PC) (Figures 3,4C, bottom), and additionally capable of capturing changes in asymmetric relationships over the scan (Figure S4).

Studying how activity or information flows between neural elements is crucial to our understanding of the mechanisms of communication. In addition to EWC, multiple previous works have explored this important topic from diverse standpoints, such as neuronal avalanches (Beggs and Plenz 2003, 2004; Sorrentino et al. 2021), direct stimulation-response measurements (Seguin et al. 2023a), functional hierarchies (Vázquez-Rodríguez et al. 2020), FC dynamics (Faskowitz et al. 2020; Griffa et al. 2017), and information-theoretic methods (Nguyen et al. 2024; Novelli et al. 2019; Novelli and Lizier 2021), to name a few. EWC differs from previous work primarily in its handling of time series. As opposed to measures/features computed using the entirety of recordings or parts of them (as in sliding window approaches), EWC restricts FC estimation to select subsamples of the signal, to infer activity propagation between neural elements. By targeting the FC estimation to select subsamples of the scan, EWC effectively computes a resting-state "event-related potential". Approaches with parallels to the EWC framework have been previously applied in epilepsy research, where activity and FC changes associated with interictal spikes were found to be informative of seizure propagation, seizure onset zones, and epileptogenic networks (Bartolomei et al. 2017; Corona et al. 2023; Matarrese et al. 2023; Van Mierlo et al. 2013; Wilke et al. 2009).

Estimating EWC comprises three steps: (1) event identification, (2) temporal ordering, (3) windowing/subsampling. Each of these elements has associated advantages and limitations. We discuss these points below.

Typically, FC is estimated for the entire scan, or in the case of dynamical-FC, for consecutive windows of the scan (Hutchison et al. 2013; Schulz and Huston 2002; Vergara et al. 2019). A limitation of such an approach to capture activity propagation is that inter-regional communication may occur only at select time epochs and this information may be obscured by internal dynamics. Although both dynamic-FC and EWC involve FC-estimation through a windowed approach, key technical differences between the methodologies include EWC's focus on salient signal features for each region, their respective window placement strategies, and the subsequent averaging of estimates over temporally separated communication windows in EWC. These algorithmic differences result in dFC and EWC capturing conceptually different aspects of interregional interactions—dFC effectively captures the temporal variation of FC over the duration of a scan, whereas EWC develops maps of dominant directed or asymmetric interactions associated with discrete activity propagation events (Figure S6).

The purpose of the event-identification step in the EWC is to identify salient features in regional dynamics that then serve as a reference point from which downstream effects are gauged. In task-based paradigms, these segments are generally marked by controlled stimulus triggers. On the other hand, in task-free recordings, change-point detection or point-process analysis-based tools can be used to capture salient changes in regional dynamics (Aminikhanghahi and Cook 2017; Chen et al. 2019; Tagliazucchi et al. 2011, 2012). EWC reuses a simple method employed in previous works that traces activity propagation to parts of the signal that deviate from mean behavior through $z$ scoring (Sorrentino et al. 2021). Limiting the signal that is analyzed to the proximity of the events additionally makes the EWC computationally tractable when compared to conventional approaches (Figure 3). Although event detection is performed on the time-domain signal, a similar approach may also be implemented in the time-frequency domain. This would be particularly suited for investigating the downstream effects of transient neural-oscillatory phenomena, such as beta bursts, whose propagation can be used to delineate functionally relevant circuits (Lundqvist et al. 2024). The event-identification function would ideally be chosen based on the neural recordings and what the researcher considers to be a valid perturbation.

The temporal ordering aspect, which is designed to account for delays in signal conduction over the network, incorporates directionality into the protocol, irrespective of the FC measure used. This allows us to use undirected/symmetric measures like PC or cMI to resolve transient asymmetric FC relationships (Figure 2B,C,E,F). Any symmetric FC measure (coherence, phase locking value, phase lag index etc. [Colclough et al. 2016; Lachaux et al. 1999; Stam et al. 2007]) can similarly be rendered directional if implemented in this manner. Care must, however, be taken to ensure that the considered delays are within a reasonable range to avoid capturing effects that might not likely be caused by the observed event.

Limiting the FC estimation to a window/subsample of the signal proximal to the events offers multiple advantages. It is well suited for scenarios where there is limited information regarding the spatiotemporal span of the effects, allowing us to capture extended effects as opposed to a local one (at a single time point). Furthermore, averaging the results over multiple windows (events) increases the robustness of the estimate. It also reduces the size of the signal for which the FC must be estimated, decreasing the computational time.

In contrast to conventional FC implementations, however, EWC typically involves a higher number of computations—instead of a single computation per epoch, there are now computations associated with each event within the epoch (albeit involving

shorter segments of data). This effect is apparent in Figure 3, where MI-Full is computed considerably faster than its EWC counterpart—cMI-EWC.

Although we find that there is a strong agreement between the subject-level PC-EWC and TE-Full, we noted that agreement in terms of their asymmetry or directionality was not statistically significant. This could be due to the PC and TE capturing different statistical dependencies in the data. This difference may have been subtle in the simple network-motif (resulting in both the PC and TE capturing the true signaling asymmetries), but more pronounced at larger scales. Additionally, we should mention that the PC and information theoretic measures such as the cMI or TE estimated using Gaussian estimators only capture linear dependencies in the data. While linear approximations are commonly used to make analytical problems tractable, the model-free nature of information theoretic measures (using model-free estimators such as the Kraskov–Stögbauer–Grassberger (KSG) or binning estimators) makes them more suitable to capture non-linear dependencies following perturbations.

An important feature of EWC is that, being a generalized time series analytical framework, it is not restricted to M/EEG analyses but can be applied to a host of functional neuroimaging modalities—from microelectrode array recordings of neural populations to functional MRI. For example, EWC could be applied to intracranial EEG (iEEG) recordings to assess the transmission of endogenous perturbations at fine spatiotemporal scales and possibly contextualize insights from stimulation-based approaches to neural communication (Lemarechal et al. 2022; Seguin et al. 2023a; Trebaul et al. 2018). As discussed above, this would, however, require that the event identification principles, delays, and window lengths suit the modality and research question. Nevertheless, a standardized analytical treatment across diverse data facilitates comparison and consolidation of insights from multiple scales, promoting a deeper understanding of a complex process like neural communication. We anticipate EWC's utility in multiple venues of research, from basic neuroscience to translation. For instance, gauging the relationship between EWC and neurophysiological factors such as neural oscillatory relationships could potentially help elucidate mechanisms or principles underlying routing of information at various scales. EWC's modality-general framework could also prove useful in the context of neural decoding, where conventional approaches involving multiple modalities and diverse associated analytical techniques are argued to provide a limited characterization of the neural code (Lu et al. 2021). By estimating statistical responses to stimulus-driven activity changes, EWC could be leveraged to capture standardized representations of stimuli across modalities and possibly complement established fusion-based approaches (Cichy et al. 2016). Another domain where we anticipate EWC's utility is in brain stimulation, to potentially characterize how stimulation modalities might modulate communication between downstream regions and influence treatment outcomes. In the context of epilepsy research, EWC might find utility in assessing the relevance of various epileptiform signal features (defined/identified as events) on ictal and interictal communication, building seizure propagation models, or validating epileptogenic mechanisms by tracking interareal interactions leading up to seizures. EWC could also be incorporated into previously developed methodologies involving neural time series for example, using feature vectors instead of raw time series (Nguyen et al. 2024).

### 4.1 | Methodological Considerations

We designed EWC to capture communication-driven statistical relationships or as a statistical analogue of activity propagation. Its development involved the use of several simplifying assumptions to ensure computational and analytical tractability. These points need to be considered to fully appreciate the scope of this work and limitations. For instance, a $z$-value-based event identification, as we used in this study, will be sensitive to changes in the mean activity—this is evident in Figure S2F, where an increase in the source firing rate results in firing events not being identified, resulting in diminished estimates. Similarly, errors in delay estimation, which affect the temporal ordering, can result in the effect of the event being missed entirely. The window length is also a crucial component and must be chosen so that it captures the immediate effects of the event, while also being long enough to ensure that there are enough datapoints for an accurate FC estimate. The window and epoch lengths also determine the resolution at which the dynamics of asymmetric relationships can be observed (event−/epoch-scale vs. subject-scale).

We use the Euclidean separation between ROI centroids as a measure of the physical separation between them, which in turn dictates the signal transmission delay and subsequent temporal ordering in EWC. While the Euclidean separation is a convenient and widely used method of incorporating signaling delays in the absence of white matter tract tracing data, delays can be better approximated by considering true white matter fibre lengths and/or accurate conduction velocities. Moreover, gauging the response of a target over a window instead of a single time point allows for slight errors in delay estimation, provided the response is not highly temporally localized.

It must also be emphasized that the inference times are subject to the methods employed for event identification and the FC measure. For instance, using PC instead of cMI reduces the overall inference time (Figure 3). On the other hand, replacing the event identification with a more complex procedure, such as identifying salient events in the time-frequency domain, can increase the overall time taken for activity propagation inference.

It is also important to remember that EWC is not a direct measure of communication but is instead a measure of the statistical consequence of communication. It can only be used to infer communication. Care must be taken while choosing the FC measure, since different measures capture different features of signal similarity (correlation, phase synchrony etc.), while also being valid only on certain derivatives of the original signal. For example, mutual information can be computed between any signal (with different interpretations), whereas the phase lag index is computed between the instantaneous phase time series. The effect of FC measure choice is evident in Figure 2B,C,E,F, where the cMI indicates strong interaction from node 4 to 2, despite the lack of any interaction by construction. The PC, on the other hand, does not capture this functional link. In the case of non-negative FC measures like the cMI, estimates can sometimes be inflated due to a positive bias (despite filtering based on significance testing).

This can be corrected by subtracting a null-derived estimate from the observed (significant) estimate. Additionally, the current EWC implementation identifies perturbations at the level of a single region (the source) and infers activity propagation between pairs of regions at a time. Our framework can be extended to multiple dimensions. Examples include defining events based on significant deviations of joint activities of multiple regions (instead of a single source) using a generalized notion of the $z$ score, or conditioning the statistical dependence between source and target on the activities of other regions.

Furthermore, we must mention that although our protocol restricts the estimation of the EWC to supra-threshold events, we do not claim that communication does not take place during the sub-threshold segments. The significant deviations are used to systematically reduce the analysis space, since it is more difficult to establish whether EWC estimates are due to communication as opposed to some other regional process or noise in the sub-threshold segments.

## 5 | Conclusion

In conclusion, our work presents a new method to infer neural communication patterns through a restricted FC estimation approach based on activity propagation events. Our method yields communication maps comparable to those of well-established techniques at a fraction of the computational time, opening up new avenues for the investigation of signaling in large networks of neural elements.


### Acknowledgments

V.M.M. is supported by the Melbourne Research Scholarship, University of Melbourne. R.F.H.C. is funded by a NHMRC Emerging Leadership Investigator Grant (Grant number: 2017527). C.S. acknowledges support from the Australian Research Council (Grant number: DP170101815). A.Z. is supported by an ARC Future Fellowship (Grant number: FT220100091) and the Rebecca L. Cooper Foundation. Data were provided (in part) by the Human Connectome Project, WU-Minn Consortium (Principal Investigators: David Van Essen and Kamil Ugurbil; 1U54MH091657) funded by the 16 NIH Institutes and Centers that support the NIH Blueprint for Neuroscience Research; and by the McDonnell Center for Systems Neuroscience at Washington University. This research was supported by The University of Melbourne's Research Computing Services and the Petascale Campus Initiative. Open access publishing facilitated by The University of Melbourne, as part of the Wiley - The University of Melbourne agreement via the Council of Australian University Librarians.


### Data Availability Statement

The data that support the findings of this study are openly available in EWC at https://github.com/vmadanmohan/EWC.

### References


Abeysuriya, R. G., J. Hadida, S. N. Sotiropoulos, et al. 2018. "A Biophysical Model of Dynamic Balancing of Excitation and Inhibition in Fast Oscillatory Large-Scale Networks." *PLoS Computational Biology* 14, no. 2: e1006007. https://doi.org/10.1371/journal.pcbi.1006007.

Aminikhanghahi, S., and D. J. Cook. 2017. "A Survey of Methods for Time Series Change Point Detection." *Knowledge and Information Systems* 51, no. 2: 339–367. https://doi.org/10.1007/s10115-016-0987-z.

Avena-Koenigsberger, A., B. Misic, and O. Sporns. 2018. "Communication Dynamics in Complex Brain Networks." *Nature Reviews Neuroscience* 19, no. 1: 17–33. https://doi.org/10.1038/nrn.2017.149.

Avena-Koenigsberger, A., X. Yan, A. Kolchinsky, M. P. Van Den Heuvel, P. Hagmann, and O. Sporns. 2019. "A Spectrum of Routing Strategies for Brain Networks." *PLoS Computational Biology* 15, no. 3: e1006833. https://doi.org/10.1371/journal.pcbi.1006833.

Barnett, L., and A. K. Seth. 2014. "The MVGC Multivariate Granger Causality Toolbox: A New Approach to Granger-Causal Inference." *Journal of Neuroscience Methods* 223: 50–68. https://doi.org/10.1016/j.jneumeth.2013.10.018.

Barnett, L., and A. K. Seth. 2015. "Granger Causality for State-Space Models." *Physical Review E: Statistical, Nonlinear, and Soft Matter Physics* 91, no. 4: 40101. https://doi.org/10.1103/PhysRevE.91.040101.

Bartolomei, F., S. Lagarde, F. Wendling, et al. 2017. "Defining Epileptogenic Networks: Contribution of SEEG and Signal Analysis." *Epilepsia* 58, no. 7: 1131–1147. https://doi.org/10.1111/epi.13791.

Bazinet, V., R. Vos de Wael, P. Hagmann, B. C. Bernhardt, and B. Misic. 2021. "Multiscale Communication in Cortico-Cortical Networks." *NeuroImage* 243: 118546. https://doi.org/10.1016/j.neuroimage.2021.118546.

Beggs, J. M., and D. Plenz. 2003. "Behavioral/Systems/Cognitive Neuronal Avalanches in Neocortical Circuits." *Journal of Neuroscience* 23, no. 35: 11167–11177.

Beggs, J. M., and D. Plenz. 2004. "Neuronal Avalanches Are Diverse and Precise Activity Patterns That Are Stable for Many Hours in Cortical Slice Cultures." *Journal of Neuroscience* 24, no. 22: 5216–5229. https://doi.org/10.1523/JNEUROSCI.0540-04.2004.

Bonnefond, M., S. Kastner, and O. Jensen. 2017. "Communication Between Brain Areas Based on Nested Oscillations." *ENeuro* 4, no. 2: 1–14. https://doi.org/10.1523/ENEURO.0153-16.2017.

Bressler, S. L., and A. K. Seth. 2011. "Wiener-Granger Causality: A Well Established Methodology." *NeuroImage* 58, no. 2: 323–329. https://doi.org/10.1016/j.neuroimage.2010.02.059.

Chapeton, J. I., R. Haque, J. H. Wittig, S. K. Inati, and K. A. Zaghloul. 2019. "Large-Scale Communication in the Human Brain is Rhythmically Modulated Through Alpha Coherence." *Current Biology* 29, no. 17: 2801–2811. https://doi.org/10.1016/j.cub.2019.07.014.

Chen, G., G. Lu, W. Shang, and Z. Xie. 2019. "Automated Change-Point Detection of EEG Signals Based on Structural Time-Series Analysis." *IEEE Access* 7: 180168–180180. https://doi.org/10.1109/ACCESS.2019.2956768.

Cichy, R. M., D. Pantazis, and A. Oliva. 2016. "Similarity-Based Fusion of MEG and fMRI Reveals Spatio-Temporal Dynamics in Human Cortex During Visual Object Recognition." *Cerebral Cortex* 26, no. 8: 3563–3579. https://doi.org/10.1093/cercor/bhw135.

Colclough, G. L., M. J. Brookes, S. M. Smith, and M. W. Woolrich. 2015. "A Symmetric Multivariate Leakage Correction for MEG Connectomes." *NeuroImage* 117: 439–448. https://doi.org/10.1016/j.neuroimage.2015.03.071.

Colclough, G. L., M. W. Woolrich, P. K. Tewarie, M. J. Brookes, A. J. Quinn, and S. M. Smith. 2016. "How Reliable are MEG Resting-State Connectivity Metrics?" *NeuroImage* 138: 284–293. https://doi.org/10.1016/j.neuroimage.2016.05.070.

Corona, L., E. Tamilia, M. Scott Perry, et al. 2023. "Non-Invasive Mapping of Epileptogenic Networks Predicts Surgical Outcome." *Brain* 146, no. 5: 1916–1931. https://doi.org/10.1093/brain/awac477.

Dale, A. M., A. K. Liu, B. R. Fischl, et al. 2000. "Dynamic Statistical Parametric Mapping: Combining fMRI and MEG for High-Resolution Imaging of Cortical Activity." *Neuron* 26: 55–67.

Deco, G., V. Jirs, A. R. McIntosh, O. Sporns, and R. Kötter. 2009. "Key Role of Coupling, Delay, and Noise in Resting Brain Fluctuations." *Proceedings of the National Academy of Sciences of the United States of America* 106, no. 25: 10302–10307. https://doi.org/10.1073/pnas.0901831106.

Faskowitz, J., F. Z. Esfahlani, Y. Jo, O. Sporns, and R. F. Betzel. 2020. "Edge-Centric Functional Network Representations of Human Cerebral Cortex Reveal Overlapping System-Level Architecture." *Nature Neuroscience* 23, no. 12: 1644–1654. https://doi.org/10.1038/s41593-020-00719-y.

Fries, P. 2005. "A Mechanism for Cognitive Dynamics: Neuronal Communication Through Neuronal Coherence." *Trends in Cognitive Sciences* 9, no. 10: 474–480. https://doi.org/10.1016/j.tics.2005.08.011.

Fries, P. 2015. "Rhythms for Cognition: Communication Through Coherence." *Neuron* 88, no. 1: 220–235. https://doi.org/10.1016/j.neuron.2015.09.034.

Friston, K. J., C. D. Frith, P. F. Liddle, and R. S. J. Frackowiak. 1993. "Functional Connectivity: The Principal-Component Analysis of Large (PET) Data Sets." *Journal of Cerebral Blood Flow and Metabolism* 13, no. 1: 5–14.

Galán, R. F. 2008. "On How Network Architecture Determines the Dominant Patterns of Spontaneous Neural Activity." *PLoS One* 3, no. 5: e2148. https://doi.org/10.1371/journal.pone.0002148.

Goñi, J., A. Avena-Koenigsberger, N. Velez de Mendizabal, M. P. van den Heuvel, R. F. Betzel, and O. Sporns. 2013. "Exploring the Morphospace of Communication Efficiency in Complex Networks." *PLoS One* 8, no. 3: e58070. https://doi.org/10.1371/journal.pone.0058070.

Granger, C. W. J. 1969. "Investigating Causal Relations by Econometric Models and Cross-Spectral Methods." *Econometrica* 37, no. 3: 424. https://doi.org/10.2307/1912791.

Griffa, A., B. Ricaud, K. Benzi, et al. 2017. "Transient Networks of Spatio-Temporal Connectivity Map Communication Pathways in Brain Functional Systems." *NeuroImage* 155: 490–502. https://doi.org/10.1016/j.neuroimage.2017.04.015.

Hahn, G., A. F. Bujan, Y. Frégnac, A. Aertsen, and A. Kumar. 2014. "Communication Through Resonance in Spiking Neuronal Networks." *PLoS Computational Biology* 10, no. 8: e1003811. https://doi.org/10.1371/journal.pcbi.1003811.

Hahn, G., A. Ponce-Alvarez, G. Deco, A. Aertsen, and A. Kumar. 2019. "Portraits of Communication in Neuronal Networks." *Nature Reviews Neuroscience* 20, no. 2: 117–127. https://doi.org/10.1038/s41583-018-0094-0.

Han, S., Q. Cui, X. Wang, et al. 2020. "Resting State Functional Network Switching Rate is Differently Altered in Bipolar Disorder and Major Depressive Disorder." *Human Brain Mapping* 41, no. 12: 3295–3304. https://doi.org/10.1002/hbm.25017.

Hansen, E. C. A., D. Battaglia, A. Spiegler, G. Deco, and V. K. Jirsa. 2015. "Functional Connectivity Dynamics: Modeling the Switching Behavior of the Resting State." *NeuroImage* 105: 525–535. https://doi.org/10.1016/j.neuroimage.2014.11.001.

Hulata, E., R. Segev, and E. Ben-Jacob. 2002. "A Method for Spike Sorting and Detection Based on Wavelet Packets and Shannon's Mutual Information." *Journal of Neuroscience Methods* 117, no. 1: 1–12. https://doi.org/10.1016/s0165-0270(02)00032-8.

Hutchison, R. M., T. Womelsdorf, E. A. Allen, et al. 2013. "Dynamic Functional Connectivity: Promise, Issues, and Interpretations." *NeuroImage* 80: 360–378. https://doi.org/10.1016/j.neuroimage.2013.05.079.

Jensen, O., and A. Mazaheri. 2010. "Shaping Functional Architecture by Oscillatory Alpha Activity: Gating by Inhibition." *Frontiers in Human Neuroscience* 4: 186. https://doi.org/10.3389/fnhum.2010.00186.

Kirst, C., M. Timme, and D. Battaglia. 2016. "Dynamic Information Routing in Complex Networks." *Nature Communications* 7: 11061. https://doi.org/10.1038/ncomms11061.

Lachaux, J. P., E. Rodriguez, J. Martinerie, and F. J. Varela. 1999. "Measuring Phase Synchrony in Brain Signals." *Human Brain Mapping* 8, no. 4: 194–208. https://doi.org/10.1002/(SICI)1097-0193(1999)8:4<194::AID-HBM4>3.0.CO;2-C.

Lemarechal, J. D., M. Jedynak, L. Trebaul, et al. 2022. "A Brain Atlas of Axonal and Synaptic Delays Based on Modelling of Cortico-Cortical Evoked Potentials." *Brain* 145, no. 5: 1653–1667. https://doi.org/10.1093/brain/awab362.

Lerner, T. N., L. Ye, and K. Deisseroth. 2016. "Communication in Neural Circuits: Tools, Opportunities, and Challenges." *Cell* 164, no. 6: 1136–1150. https://doi.org/10.1016/j.cell.2016.02.027.

Lizier, J. T. 2014. "JIDT: An Information-Theoretic Toolkit for Studying the Dynamics of Complex Systems." *Frontiers in Robotics and AI* 1: 1–20. https://doi.org/10.3389/frobt.2014.00011.

Lu, H. Y., E. S. Lorenc, H. Zhu, et al. 2021. "Multi-scale neural decoding and analysis." *Journal of Neural Engineering* 18, no. 4: 45013. https://doi.org/10.1088/1741-2552/ac160f.

Lundqvist, M., E. K. Miller, J. Nordmark, J. Liljefors, and P. Herman. 2024. "Beta: Bursts of Cognition." *Trends in Cognitive Sciences* 28, no. 7: 662–676. https://doi.org/10.1016/j.tics.2024.03.010.

Lynall, M. E., D. S. Bassett, R. Kerwin, et al. 2010. "Functional Connectivity and Brain Networks in Schizophrenia." *Journal of Neuroscience* 30, no. 28: 9477–9487. https://doi.org/10.1523/JNEUROSCI.0333-10.2010.

Matarrese, M. A. G., A. Loppini, L. Fabbri, et al. 2023. "Spike Propagation Mapping Reveals Effective Connectivity and Predicts Surgical Outcome in Epilepsy." *Brain* 146, no. 9: 3898–3912. https://doi.org/10.1093/brain/awad118.

Mitra, A., and M. E. Raichle. 2016. "How Networks Communicate: Propagation Patterns in Spontaneous Brain Activity." *Philosophical Transactions of the Royal Society, B: Biological Sciences* 371, no. 1705: 20150546. https://doi.org/10.1098/rstb.2015.0546.

Nguyen, A., O. McMullin, J. T. Lizier, and B. D. Fulcher. 2024. "A Feature-Based Information-Theoretic Approach for Detecting Interpretable, Long-Timescale Pairwise Interactions From Time Series". arxiv 2404.05929.

Niso, G., F. Tadel, E. Bock, M. Cousineau, A. Santos, and S. Baillet. 2019. "Brainstorm Pipeline Analysis of Resting-State Data From the Open MEG Archive." *Frontiers in Neuroscience* 13, no. APR: 284. https://doi.org/10.3389/fnins.2019.00284.

Novelli, L., and J. T. Lizier. 2021. "Inferring Network Properties From Time Series Using Transfer Entropy and Mutual Information: Validation of Multivariate Versus Bivariate Approaches." *Network Neuroscience* 5, no. 2: 373–404. https://doi.org/10.1162/netn_a_00178.

Novelli, L., P. Wollstadt, P. Mediano, M. Wibral, and J. T. Lizier. 2019. "Large-Scale Directed Network Inference With Multivariate Transfer Entropy and Hierarchical Statistical Testing." *Network Neuroscience* 3, no. 3: 827–847. https://doi.org/10.1162/netn_a_00092.

O'Neill, G. C., P. K. Tewarie, G. L. Colclough, et al. 2017. "Measurement of Dynamic Task Related Functional Networks Using MEG." *NeuroImage* 146: 667–678. https://doi.org/10.1016/j.neuroimage.2016.08.061.

Palmigiano, A., T. Geisel, F. Wolf, and D. Battaglia. 2017. "Flexible Information Routing by Transient Synchrony." *Nature Neuroscience* 20, no. 7: 1014–1022. https://doi.org/10.1038/nn.4569.

Palus, M. 1997. "Detecting Phase Synchronization in Noisy Systems." *Physics Letters A* 235, no. 4: 341–351.

Papadopoulos, L., C. W. Lynn, D. Battaglia, and D. S. Bassett. 2020. "Relations Between Large-Scale Brain Connectivity and Effects of

Regional Stimulation Depend on Collective Dynamical State." *PLoS Computational Biology* 16, no. 9: e1008144. https://doi.org/10.1371/journal.pcbi.1008144.

Quinn, A. J., M. W. J. van Es, C. Gohil, and M. W. Woolrich. 2023. OHBA Software Library in Python (OSL) (0.2.0).

Schaefer, A., R. Kong, E. M. Gordon, et al. 2018. "Local-Global Parcellation of the Human Cerebral Cortex From Intrinsic Functional Connectivity MRI." *Cerebral Cortex* 28, no. 9: 3095–3114. https://doi.org/10.1093/cercor/bhx179.

Schipul, S. E., T. A. Keller, and M. A. Just. 2011. "Inter-Regional Brain Communication and Its Disturbance in Autism." *Frontiers in Systems Neuroscience* 5: 1–11. https://doi.org/10.3389/fnsys.2011.00010.

Schnitzler, A., and J. Gross. 2005. "Normal and Pathological Oscillatory Communication in the Brain." *Nature Reviews Neuroscience* 6, no. 4: 285–296. https://doi.org/10.1038/nrn1650.

Schreiber, T. 2000. "Measuring Information Transfer." *Physical Review Letters* 85, no. 2: 461–464.

Schulz, D., and J. P. Huston. 2002. "The Sliding Window Correlation Procedure for Detecting Hidden Correlations: Existence of Behavioral Subgroups Illustrated With Aged Rats." *Journal of Neuroscience Methods* 121: 129–137.

Seguin, C., M. Jedynak, O. David, S. Mansour, O. Sporns, and A. Zalesky. 2023a. "Communication Dynamics in the Human Connectome Shape the Cortex-Wide Propagation of Direct Electrical Stimulation." *Neuron* 111: 1391–1401. https://doi.org/10.1016/j.neuron.2023.01.027.

Seguin, C., O. Sporns, and A. Zalesky. 2023b. "Brain Network Communication: Concepts, Models and Applications." *Nature Reviews. Neuroscience* 24: 557–574. https://doi.org/10.1038/s41583-023-00718-5.

Seguin, C., M. P. Van Den Heuvel, and A. Zalesky. 2018. "Navigation of Brain Networks." *Proceedings of the National Academy of Sciences of the United States of America* 115, no. 24: 6297–6302. https://doi.org/10.1073/pnas.1801351115.

Shafiei, G., S. Baillet, and B. Misic. 2022. "Human Electromagnetic and Haemodynamic Networks Systematically Converge in Unimodal Cortex and Diverge in Transmodal Cortex." *PLoS Biology* 20, no. 8: e3001735. https://doi.org/10.1371/journal.pbio.3001735.

Shorten, D. P., R. E. Spinney, and J. T. Lizier. 2021. "Estimating Transfer Entropy in Continuous Time Between Neural Spike Trains or Other Event-Based Data." *PLoS Computational Biology* 17, no. 4: e1008054. https://doi.org/10.1371/journal.pcbi.1008054.

Shriki, O., J. Alstott, F. Carver, et al. 2013. "Neuronal Avalanches in the Resting MEG of the Human Brain." *Journal of Neuroscience* 33, no. 16: 7079–7090. https://doi.org/10.1523/JNEUROSCI.4286-12.2013.

Sorrentino, P., C. Seguin, R. Rucco, et al. 2021. "The Structural Connectome Constrains Fast Brain Dynamics." *eLife* 10: 1–11. https://doi.org/10.7554/eLife.67400.

Stam, C. J., G. Nolte, and A. Daffertshofer. 2007. "Phase Lag Index: Assessment of Functional Connectivity From Multi Channel EEG and MEG With Diminished Bias From Common Sources." *Human Brain Mapping* 28, no. 11: 1178–1193. https://doi.org/10.1002/hbm.20346.

Suárez, L. E., R. D. Markello, R. F. Betzel, and B. Misic. 2020. "Linking Structure and Function in Macroscale Brain Networks." *Trends in Cognitive Sciences* 24, no. 4: 302–315. https://doi.org/10.1016/j.tics.2020.01.008.

Tadel, F., S. Baillet, J. C. Mosher, D. Pantazis, and R. M. Leahy. 2011. "Brainstorm: A User-Friendly Application for MEG/EEG Analysis." *Computational Intelligence and Neuroscience* 2011: 879716. https://doi.org/10.1155/2011/879716.

Tagliazucchi, E., P. Balenzuela, D. Fraiman, and D. R. Chialvo. 2012. "Criticality in Large-Scale Brain Fmri Dynamics Unveiled by a Novel Point Process Analysis." *Frontiers in Physiology* 3: 15. https://doi.org/10.3389/fphys.2012.00015.

Tagliazucchi, E., P. Balenzuela, D. Fraiman, P. Montoya, and D. R. Chialvo. 2011. "Spontaneous BOLD Event Triggered Averages for Estimating Functional Connectivity at Resting State." *Neuroscience Letters* 488, no. 2: 158–163. https://doi.org/10.1016/j.neulet.2010.11.020.

The MathWorks Inc. 2022. *MATLAB version: 9.13.0 (R2022b)*. MathWorks Inc.

Trebaul, L., P. Deman, V. Tuyisenge, et al. 2018. "Probabilistic Functional Tractography of the Human Cortex Revisited." *NeuroImage* 181: 414–429. https://doi.org/10.1016/j.neuroimage.2018.07.039.

Uusitalo, M. A., and R. J. Ilmoniemi. 1997. "Signal-Space Projection Method for Separating MEG or EEG Into Components." *Medical and Biological Engineering and Computing* 35: 135–140.

Van Essen, D. C., S. M. Smith, D. M. Barch, T. E. J. Behrens, E. Yacoub, and K. Ugurbil. 2013. "The WU-Minn Human Connectome Project: An Overview." *NeuroImage* 80: 62–79. https://doi.org/10.1016/j.neuroimage.2013.05.041.

Van Mierlo, P., E. Carrette, H. Hallez, et al. 2013. "Ictal-Onset Localization Through Connectivity Analysis of Intracranial EEG Signals in Patients With Refractory Epilepsy." *Epilepsia* 54, no. 8: 1409–1418. https://doi.org/10.1111/epi.12206.

Vázquez-Rodríguez, B., Z. Q. Liu, P. Hagmann, and B. Misic. 2020. "Signal propagation via cortical hierarchies." *Network Neuroscience* 4, no. 4: 1072–1090. https://doi.org/10.1162/netn_a_00153.

Vergara, V. M., A. Abrol, and V. D. Calhoun. 2019. "An Average Sliding Window Correlation Method for Dynamic Functional Connectivity." *Human Brain Mapping* 40, no. 7: 2089–2103. https://doi.org/10.1002/hbm.24509.

Wilke, C., W. van Drongelen, M. Kohrman, and B. He. 2009. "Identification of Epileptogenic Foci From Causal Analysis of ECoG Interictal Spike Activity." *Clinical Neurophysiology* 120, no. 8: 1449–1456. https://doi.org/10.1016/j.clinph.2009.04.024.

Wilmer, A., M. de Lussanet, and M. Lappe. 2012. "Time-Delayed Mutual Information of the Phase as a Measure of Functional Connectivity." *PLoS One* 7, no. 9: e44633. https://doi.org/10.1371/journal.pone.0044633.

**Supporting Information**

Additional supporting information can be found online in the Supporting Information section.